Nonlinear dynamics of resonant interactions between wave packets and particle distributions with loss-cone-like structures

C. Krafft,[1,2] A. Volokitin,[3] and A. Zaslavsky[4]
[1]*Laboratoire de Physique des Plasmas, Ecole Polytechnique, 91128 Palaiseau Cedex, France*
[2]*Paris South University, 91405 Orsay Cedex, France*
[3]*Space Research Institute (IKI), 84/32 Profsoyuznaya Str., Moscow 117997, Russia*
[4]*LESIA, Observatoire de Paris, 92195 Meudon Cedex, France*
(Received 2 April 2010; revised manuscript received 15 October 2010; published 2 December 2010)

The paper studies the nonlinear mechanisms at work in magnetized plasmas when wave packets interact resonantly with particle distributions presenting loss-cone-like structures. Lower hybrid waves are considered in view of the great importance, in space and laboratory plasmas, of waves with frequencies below the electron cyclotron frequency. Owing to a three-dimensional Hamiltonian model and a numerical symplectic code, the authors study the nonlinear stage of the loss-cone instability for various particle distributions and wave spectra involving symmetric and asymmetric features. In particular, the wave-particle interaction process of dynamical resonance merging, which results from an instability of the trapped particles' motion and leads to complex stochastic phenomena, is discussed. Whereas interactions at normal cyclotron resonances are mostly considered, the role of the Landau and the anomalous cyclotron resonances is also studied to explain thoroughly the nonlinear wave-particle dynamics as well as the competition between loss-cone, fan, and beam instabilities. The relaxed particle distributions and the saturated wave spectra are analyzed. The time necessary for filling the loss-cone structures is determined as a function of the characteristics of the particle distributions. Whereas most of the previous works analyzed the asymptotic stage of the system's evolution in the frame of the well-known quasilinear theory, the paper considers the case when the energy carried by the wave packet is sufficiently large so that the description of the physical processes at work cannot be limited to the frame of weak turbulence theories.

DOI: 10.1103/PhysRevE.82.066402 PACS number(s): 52.35.Mw

I. INTRODUCTION

Particle velocity distributions presenting loss-cone-like structures can be encountered in various space and laboratory plasmas as, for example, planetary magnetospheres, solar and stellar atmospheres, or plasma containment experiments [1–6]. Such nonequilibrium distributions typically arise when a plasma is confined in a magnetic bottle where particles are trapped locally and bounce back and forth between mirror points, being reflected by the converging magnetic field lines. They can drive so-called loss-cone instabilities that are responsible for important linear and nonlinear phenomena in magnetized plasmas [1–10] as, for example, in experiments with confinement in "open-ended" containment fields (e.g., mirror machines [1]) or in the earth ionized surrounding, notably in the auroral regions, where ion and electron fluxes with loss-cone-like structures are commonly observed by satellites [2–4]. Let us cite among others the observations recorded by the *Ulysses* spacecraft in the solar wind that reveal the existence of suprathermal electron distributions with loss-cone features [5] and, more recently, by the *Wind* spacecraft that report the simultaneous presence of whistlers very well time correlated with Langmuir waves and loss-cone electron distributions [6].

Although both electron and ion velocity distributions can present loss-cone structures, the paper is focused on instabilities driven by electrons. Early studies have shown that nonrelativistic electron distributions $f_e(v_z, v_\perp)$ vanishing near the perpendicular velocity $v_\perp = 0$ could excite electrostatic waves propagating obliquely with respect to the ambient magnetic field $\mathbf{B}_0$ [7]. Linear studies concerning wave excitation by loss-cone structures were performed owing to analytical developments and numerical computations, for various types of particle distributions and waves, including or not relativistic effects [11–18]. More recently, the authors presented theoretical results and simulations [19] on the interactions of electrostatic waves with electron fluxes at normal cyclotron resonances. In particular, the linear and the nonlinear stages of the loss-cone instability mechanisms were investigated thoroughly for a single and a few waves (discrete wave spectrum).

In the present paper, the main attention is paid to study the nonlinear mechanisms at work when many waves forming dense and almost continuous spectra interact resonantly with particle distributions presenting loss-cone-like structures. The question is to investigate the nonlinear stage of the loss-cone instability as the result of wave-particle interactions at cyclotron and Landau resonances and, in particular, the physical mechanisms governing the relaxation of the particle distributions and the saturation of the wave spectra. To our knowledge, these topics have not been solved up to now. The difficulties inherent in such problems require obviously to perform numerical simulations. But to date most of them have been focused on the nonlinear processes at work when the anisotropy of the particle velocity distributions leads to the so-called cyclotron maser instability [20–27] and only few works were devoted to simulations of wave instabilities in anisotropic plasmas presenting loss-cone-like structures and negligible relativistic effects [28–31]. However, nonrelativistic electron populations which exist in space plasmas

often present positive gradients in their perpendicular velocity distributions ($\partial f_e/\partial v_\perp > 0$) and can excite intense electrostatic waves. In particular, such waves can be destabilized by loss-cone-like distributions [32–34]. Therefore we focus our study on loss-cone instabilities involving nonrelativistic particle interactions with finite amplitude waves of wide and dense spectra.

The nonlinear mechanisms governing the interactions between electromagnetic whistler waves or electrostatic lower hybrid waves and loss-cone particle distributions in magnetized plasmas are of great importance if one considers the major role that waves of frequency below the electron cyclotron frequency ω_c are playing in space and laboratory plasmas. Moreover note that, for waves with frequencies $\omega < \omega_c$ propagating oblique to $\mathbf{B}_0$, as whistlers and lower hybrid waves (which are considered in the present paper), it is possible to neglect the dependence of $\gamma=(1-v^2/c^2)^{-1/2}$ on the velocity v in the resonance condition $\omega - n\omega_c/\gamma = k_z v_z$ (k_z and v_z are the wave vector and the particle velocity along $\mathbf{B}_0$) and to consider nonrelativistic loss-cone instabilities, especially if $k_z \delta v_z \simeq \gamma_{\mathbf{k}} \gg n\omega_c v \delta v/c^2$, where δv and δv_z are the modulus and the parallel component of $\delta \mathbf{v}$, which is the variation in the velocity of the particle during its interaction with the wave, and supposing that the resonance width is of the order of the linear growth rate $\gamma_{\mathbf{k}}$.

Our study is performed by means of a self-consistent Hamiltonian model, which describes the three-dimensional (3D) dynamics of resonant interactions between wave packets and nonequilibrium particle distributions in magnetized plasmas, and a corresponding numerical symplectic code that already provided interesting results [19,35–39] in what concerns the linear and nonlinear stages of the fan and the beam instabilities at the anomalous cyclotron and Landau resonances. The paper is mainly focused on the nonlinear stage of the loss-cone instability, considering wave packets of various characteristics and typical particle distributions: the single-sided loss-cone, the doubled-sided loss-cone, and the Maxwellian with loss-cone distributions; each of them allows one to take simultaneously into account various kinds of wave-particle interaction resonances and mechanisms.

One essential aspect of our approach [19,35–37] consists in dividing the plasma in two groups of particles: a thermal bulk, which governs the dispersion of the waves, and the resonant electrons, of much smaller density than the bulk, which are responsible for the wave-particle interactions involving significant transfers of momentum and energy; only these electrons are considered in our simulations so that the computing time and the numerical noise are reduced crucially (compared to usual particle-in-cell simulations), meanwhile clearly interpretable results are obtained. Hereafter we consider first the case of two waves; in particular, a complex wave-particle interaction process, so-called "dynamical merging of resonances" [36], is discussed, which results from an instability of the trapped particles' motion, leading, in its amplification stage, to a significant growth of the waves' amplitudes and to the appearance of multitrapping phenomena [37]. Then the problem is generalized to many waves: the dynamics of wave packets interacting resonantly with loss-cone structures is studied, considering wave and particle distributions with various symmetric and asymmetric features. In this case, most of the particles involved in the resonant interactions perform complex oscillatory motions which cannot be fully described in the frame of the well-known quasilinear theory [37,40,41]. Moreover, the authors estimate analytically, as well as owing to numerical simulations, the time necessary for filling the loss-cone structures, as a function of the characteristics of the particle distributions considered. Note that in the previous works dealing with the relativistic cyclotron maser instability [20–27], the stage of the wave saturation by loss-cone-like distributions was mainly studied in the frame of the quasilinear theory [22,27], whereas our paper considers the case when the energy carried by the wave packet is sufficiently large so that the description of the physical processes at work cannot be limited to the frame of weak turbulence theories.

Note that several new physical aspects are discussed in the paper. Our previous works [35–39] were focused on the nonlinear interaction processes between wave spectra and fluxes or beams of energetic particles at Landau and anomalous cyclotron resonances, in the frame of beam and fan instabilities. Here, interactions at normal cyclotron resonances involving electron velocity distributions with loss cone-type structures and dense wave spectra are considered, for which energy and momentum exchanges are quite different, so that the nonlinear system's evolution is unlike, even if similar fundamental processes as dynamical merging occur. Moreover the simultaneous competition between the three types of interaction resonances are studied, that is, the Landau, the normal and the anomalous cyclotron resonances. Finally, the dependence of some specific features of the loss cone-type structures and the wave spectra on the nonlinear system's dynamics is examined, notably the influence of asymmetries with respect to the ambient magnetic field.

II. HAMILTONIAN MODEL AND SYMPLECTIC CODE

The analytical developments and the numerical simulations discussed below are based on a self-consistent three-dimensional Hamiltonian model [35–37] which describes the dynamics of electrostatic waves interacting resonantly with charged particles in a magnetized plasma (nonlinear wave-wave interactions are neglected compared to wave-particle ones). In this model, we suppose that the plasma electrons can be divided in two groups: a thermal bulk of density n_0 and a nonequilibrium distribution of resonant particles with a much smaller average density, $n_{res} \ll n_0$. The thermal component determines the waves' dispersion and is described in the linear approximation using hydrodynamic equations. However, the resonant particles have to be considered owing to a kinetic approach which takes into account their full nonlinear dynamics in the waves' fields.

For electrostatic oscillations in a homogeneous magnetized plasma, the electric field $\mathbf{E}$ is derived from the scalar potential $\varphi(\mathbf{r},t)=\mathrm{Re}\,\Sigma_{\mathbf{k}}\varphi_{\mathbf{k}}(t)\exp(i\mathbf{k}\cdot\mathbf{r}-i\omega_{\mathbf{k}}t)$ which consists in the superposition of plane waves with slowly varying amplitudes $\varphi_{\mathbf{k}}(t)$ so that the average electric field energy density for the wave $(\omega_{\mathbf{k}},\mathbf{k})$ is given by $\langle E_{\mathbf{k}}^2/8\pi\rangle = |\mathbf{k}\varphi_{\mathbf{k}}|^2/16\pi$; $\omega_{\mathbf{k}}$ is the frequency of the wave with Fourier component $E_{\mathbf{k}}$ and

wave vector $\mathbf{k}$. The wave-particle system can be described by the following Hamiltonian [16,35–37]:

$$H=\sum_{p=1}^{N}\left(\frac{(\mathbf{P}_p+e\mathbf{A}_0(\mathbf{r}_p)/c)^2}{2m_e}-e\,\mathrm{Re}\sum_{\mathbf{k}}\varphi_{\mathbf{k}}e^{i(\mathbf{k}\cdot\mathbf{r}_p-\omega_{\mathbf{k}}t)}\right)+V\sum_{\mathbf{k}}\omega_{\mathbf{k}}\frac{\partial\varepsilon_{\mathbf{k}}}{\partial\omega_{\mathbf{k}}}\frac{|\mathbf{k}\varphi_{\mathbf{k}}|^2}{16\pi},\tag{1}$$

where $\mathbf{P}_p=m_e\mathbf{v}_p-e\mathbf{A}_0(\mathbf{r}_p)/c$ is the generalized particle momentum, $\mathbf{r}_p$ $(\mathbf{r}_{\perp p},z_p)$ and $\mathbf{v}_p(\mathbf{v}_{\perp p},v_{zp})$ are the position and the velocity of the particle p, $\mathbf{A}_0(\mathbf{r}_p)=(\mathbf{B}_0\times\mathbf{r}_p)/2$ is the vector potential and $\mathbf{B}_0=B_0\mathbf{z}$ is the constant ambient magnetic field, directed along the axis $\mathbf{z}$; $-e<0$ and m_e are the electron charge and mass, respectively; c is the speed of light; $\varepsilon_{\mathbf{k}}=\varepsilon(\mathbf{k},\omega_{\mathbf{k}})$ is the dielectric permittivity constant for electrostatic waves in a cold magnetized plasma; $\mathbf{k}(\mathbf{k}_\perp,k_z)$ is the wave vector, where k_z and $\mathbf{k}_\perp$ are the wave vectors along to and across $\mathbf{B}_0$; V is the volume occupied by the wave-particle system; N is the number of resonant particles of density n_{res} inside the volume V.

The conservation of the total energy H and parallel momentum P_z is given by

$$H=cst,\quad P_z=\sum_p m_e v_{zp}+V\sum_{\mathbf{k}}\frac{k_z}{\omega_{\mathbf{k}}}W_{\mathbf{k}}=cst,\tag{2}$$

where the total energy density of the electrostatic waves is

$$\sum_{\mathbf{k}}W_{\mathbf{k}}=\sum_{\mathbf{k}}\omega_{\mathbf{k}}\frac{\partial\varepsilon_{\mathbf{k}}}{\partial\omega_{\mathbf{k}}}\frac{|\mathbf{k}\varphi_{\mathbf{k}}|^2}{16\pi}.\tag{3}$$

Using the Newton and the Poisson equations as well as the Liouville theorem, which allows one to express the integral over the phase space volume by the sum on the N resonant particles located in the volume $V=L_zL_\perp^2$, according to

$$\int_V\frac{d^2rdz}{L_zL_\perp^2}\int d\mathbf{v}f_{res}(\mathbf{v},\mathbf{r},t)e^{i(\omega_{\mathbf{k}}t-\mathbf{k}\cdot\mathbf{r})}\to\frac{1}{N}\sum_{p=1}^{N}e^{i(\omega_{\mathbf{k}}t-\mathbf{k}\cdot\mathbf{r}_p)},\tag{4}$$

we obtain the quasilinear equation for the time evolution of the wave potentials as

$$\frac{d}{dt}\frac{e\varphi_{\mathbf{k}}}{m_e}\simeq i\frac{2\omega_p^2}{|\mathbf{k}|^2}\left(\frac{\partial\varepsilon_{\mathbf{k}}}{\partial\omega_{\mathbf{k}}}\right)^{-1}\frac{n_{res}}{n_0}\frac{1}{N}\sum_{p=1}^{N}e^{i(\omega_{\mathbf{k}}t-\mathbf{k}\cdot\mathbf{r}_p)}.\tag{5}$$

The average density of the resonant electrons is $n_{res}=\int f_{res}(\mathbf{v},\mathbf{r},t)d\mathbf{v}d\mathbf{r}$, where $f_{res}(\mathbf{v},\mathbf{r},t)$ is the corresponding distribution function; n_0 is the background plasma density.

Equation (5) is solved self-consistently with the motion of each particle

$$\frac{d\mathbf{v}_p}{dt}+(\mathbf{v}_p\times\mathbf{z})\omega_c=\mathrm{Re}\frac{ie}{m_e}\sum_{\mathbf{k}}\mathbf{k}\varphi_{\mathbf{k}}e^{i(\mathbf{k}\cdot\mathbf{r}_p-\omega_{\mathbf{k}}t)},\quad\frac{d\mathbf{r}_p}{dt}=\mathbf{v}_p,\tag{6}$$

where $\omega_p=(4\pi n_0e^2/m_e)^{1/2}$ and $\omega_c=eB_0/m_ec$ are the electron plasma and cyclotron frequencies, respectively.

Dimensionless variables will be used in the next sections (in the text as well as in the figures) according to the normalization $\omega_{\mathbf{k}}/\omega_c$, $\omega_ct/2\pi$, $\mathbf{v}/v_*$, $\mathbf{k}v_*/\omega_c$, and $e\varphi_{\mathbf{k}}/m_ev_*^2$, where v_* is an arbitrary velocity. Then, Eq. (5) can be presented in normalized variables as

$$\frac{d}{dt}\varphi_{\mathbf{k}}\simeq i\frac{p\omega_{\mathbf{k}}}{|\mathbf{k}|^2}\frac{1}{N}\sum_{p=1}^{N}e^{i(\omega_{\mathbf{k}}t-\mathbf{k}\cdot\mathbf{r}_p)},\tag{7}$$

where p is a dimensionless parameter which characterizes the intensity of the wave-particle interaction

$$p=\frac{2\omega_p^2}{\omega_c^2\omega_{\mathbf{k}}}\left(\frac{\partial\varepsilon_{\mathbf{k}}}{\partial\omega_{\mathbf{k}}}\right)^{-1}\frac{n_{res}}{n_0}.\tag{8}$$

For lower hybrid waves, which propagate in the frequency range $\omega_{lh}=\omega_{pi}\omega_c/(\omega_c^2+\omega_p^2)^{1/2}\ll\omega_{\mathbf{k}}\le\omega_c$ (at arbitrary ω_c/ω_p) with the approximate dispersion relation

$$\frac{\omega_{\mathbf{k}}^2}{\omega_c^2}\simeq\frac{\omega_p^2}{\omega_c^2+\omega_p^2}\frac{k_z^2}{\mathbf{k}^2},\tag{9}$$

where ω_{lh} and ω_{pi} are the lower hybrid and the ion plasma frequencies, the interaction intensity is given by

$$p=\frac{\omega_p^2}{\omega_c^2+\omega_p^2}\frac{n_{res}}{n_0}\ll1,\tag{10}$$

where the derivative of the dielectric constant of lower hybrid waves, $\partial\varepsilon_{\mathbf{k}}/\partial\omega_{\mathbf{k}}=2(\omega_c^2+\omega_p^2)/\omega_c^2\omega_{\mathbf{k}}$, has been used.

These waves can be destabilized by particle distributions at the resonance conditions $v_{zn}=(\omega_{\mathbf{k}}-n\omega_c)/k_z$, where n is the harmonic number and v_{zn} is the corresponding resonant velocity; the loss-cone instability results from wave-particle interactions at the normal cyclotron resonances $n\ge1$ [for the most intense resonance, $n=1$, we use below the notation $v_{z1}=(\omega_{\mathbf{k}}-\omega_c)/k_z$].

For one wave with fixed amplitude one can show that [36,42]

$$K=m_e(v_\perp^2/2\omega_c-nv_z/k_z)=cst\tag{11}$$

is an integral of the motion for each particle (v_z and $v_\perp$ are the velocity components along to and across $\mathbf{B}_0$). This condition is fulfilled with a good enough accuracy in many cases involving two and more waves with slowly varying amplitudes, such as those considered below. Indeed, our numerical simulations show that when the wave amplitudes are growing up to some significant levels, the constant of motion holds.

Owing to the Hamiltonian structure of the model, the numerical simulations have been performed using a symplectic mover [35,39] with normalized time steps $\omega_c\Delta t\simeq0.1$–$0.2$, whereas checking the accuracy of the calculations by monitoring the H and P_z conservations (2). The symplectic property guarantees the preservation of the phase space volumes of the system. As one can separate the Hamiltonian (1) as $H=H_1+H_2$, where $H_1=\Sigma_{p=1}^N(\mathbf{P}_p+e\mathbf{A}_0(\mathbf{r}_p)/c)^2/2m_e$, the symplectic operator [43,44] $L(\Delta t)=L_1(\Delta t/2)L_2(\Delta t)L_1(\Delta t/2)+o((\Delta t)^3)$ of order 2 in time step can be used for advancing the Hamiltonian H; L_1 and L_2 are canonical transformations applying to H_1 and H_2, respectively.

The transformation L_1 acts on the normalized particles' coordinates and velocities as $\mathbf{r}_p'=\mathbf{r}_p+\hat{T}_{\mathbf{r}}\mathbf{v}_p$ and $\mathbf{v}_p'=\hat{T}_{\mathbf{v}}\mathbf{v}_p$, with

the following nonvanishing matrix elements: $\hat{T}_{\mathbf{r}11}=\hat{T}_{\mathbf{r}22}=\sin\Delta\tau$, $\hat{T}_{\mathbf{r}33}=\Delta\tau$, $\hat{T}_{\mathbf{r}12}=-\hat{T}_{\mathbf{r}21}=\cos\Delta\tau-1$ and $\hat{T}_{\mathbf{v}11}=\hat{T}_{\mathbf{v}22}=\cos\Delta\tau$, $\hat{T}_{\mathbf{v}33}=1$, $\hat{T}_{\mathbf{v}12}=-\hat{T}_{\mathbf{v}21}=-\sin\Delta\tau$, where $\Delta\tau=\omega_c\Delta t$.

The transformation L_2 for the particles' velocities $\mathbf{v}_p$ and the waves' normal amplitudes $C_{\mathbf{k}}$ is performed keeping constant positions $\mathbf{r}_p$; it can be presented as follows ($\omega_{\mathbf{k}}$, $\mathbf{k}$, and $C_{\mathbf{k}}$ are normalized values): $C'_{\mathbf{k}}=C_{\mathbf{k}}+\Delta C_{\mathbf{k}}$ and $\mathbf{v}'_p=\mathbf{v}_p-\Sigma_{\mathbf{k}}\omega_{\mathbf{k}}\mathbf{k}[\mathrm{Im}(\bar{C}_{\mathbf{k}}e^{i\mathbf{k}\cdot\mathbf{r}_p})\Delta\tau+\mathrm{Re}(\Delta C_{\mathbf{k}}e^{i\mathbf{k}\cdot\mathbf{r}_p})/\omega_{\mathbf{k}}]$, with $\bar{C}_{\mathbf{k}}=\Sigma_p e^{-i\mathbf{k}\cdot\mathbf{r}_p}$ and $\Delta C_{\mathbf{k}}=(C_{\mathbf{k}}-\bar{C}_{\mathbf{k}})(e^{-i\omega_{\mathbf{k}}\Delta\tau}-1)$.

The model allows to choose arbitrary sets of waves $(\mathbf{k},\omega_{\mathbf{k}})$ for which the periodicity conditions have to be verified, i.e., $k_{x,y,z}L_{x,y,z}/2\pi=\pm1,\pm2\ldots$, where $[L_x,L_y,L_z]$ is a 3D spatial simulation box of volume $V=L_xL_yL_z$. Initially the resonant particles are randomly distributed within the box with the same probability to occupy any position. The system is supposed to be periodic in space.

The initial velocity distribution of the resonant electrons is modeled by loss-cone functions of the type

$$f_e(v_z,v_\perp)=f_0(v_z^2+v_\perp^2)\Theta(v_\perp^2-v_z^2\tan^2\theta_{lc})/C,\quad C=\cos\theta_{lc}, \tag{12}$$

where $f_0(v^2)=\pi^{-3/2}v_{th}^{-3}e^{-v^2/v_{th}^2}$ is a Maxwellian with thermal velocity v_{th}; θ_{lc} is the so-called loss-cone angle; Θ is a more or less sharp Heaviside-type function.

III. DYNAMICAL RESONANCE MERGING

In previous works [35–37] the authors have shown, considering the case of a wave packet destabilized by energetic electron fluxes at anomalous cyclotron resonances $n\leq-1$ through the fan instability, that a nonlinear process, occurring after wave saturation due to particle trapping is fulfilled, may cause the waves to gain significant energy and the particle fluxes to relax asymptotically to a "quasilinear" distribution which is reached when the growth rates of the waves tend to zero. This nonlinear process, so-called "dynamical merging of resonances" by the authors [36], is connected with some instability of the motion of the particles trapped in the potential well of a wave due to the presence of the other waves. This instability leads to a significant increase in the waves' amplitudes and thus to the widening of their resonant velocity widths; finally it is completed when these resonant domains effectively overlap, forming complex potential structures where the particles encounter multitrapping processes [37].

Nevertheless, the understanding of the mechanisms governing this nonlinear instability remains to date incomplete; notably, the exact growth rates and instability thresholds have still to be determined as a function of the interaction parameter p [Eq. (10)] and the nature of the resonant interaction. Here our aim is to show and explain how such process develops in the case of the loss-cone instability, and under what physical conditions it can occur; although it has been observed for many waves (see the next section), we discuss hereafter, for simplicity, the case of two waves.

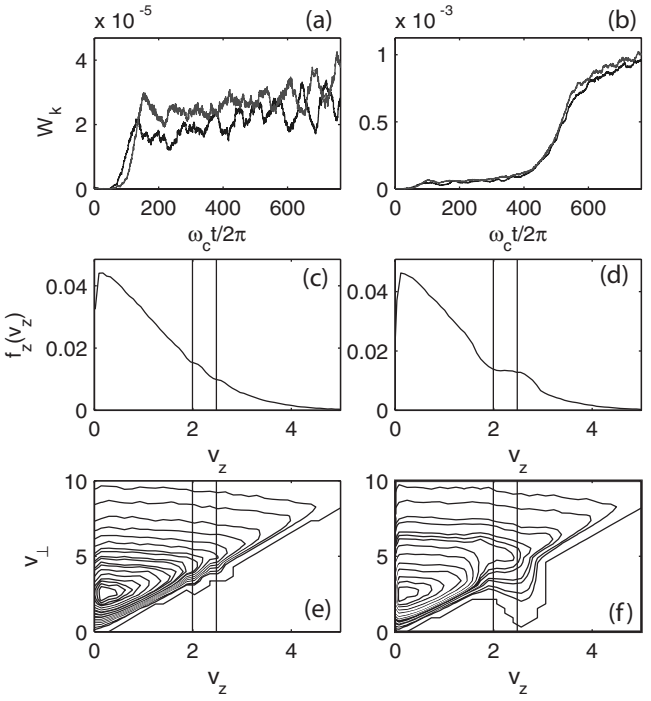

FIG. 1. Dynamical merging of resonances: interaction of two lower hybrid waves $(\mathbf{k}_1,\omega_{\mathbf{k}1})$ and $(\mathbf{k}_2,\omega_{\mathbf{k}2})$ with a loss-cone particle distribution $f_e(v_z,v_\perp)$ [Eq. (12)] at $n=1$ resonances. [(a), (c), and (e)] $p=0.02$ and no merging occurs; [(b), (d), and (f)] $p=0.025$ and the merging process develops. [(a) and (b)] evolution of the energy $W_{\mathbf{k}}\propto|E_{\mathbf{k}}|^2$ of both waves as a function of the normalized time $\omega_c t/2\pi$; [(c) and (d)] parallel velocity distribution $f_z(v_z)=\int_0^\infty 2\pi f_e(v_z,v_\perp)v_\perp dv_\perp$, at $\omega_c t/2\pi\simeq800$; [(e) and (f)] contour lines of $f_e(v_z,v_\perp)$, at $\omega_c t/2\pi\simeq800$. The vertical lines in (c)–(f) represent the resonant velocities $v_{z1,1}$ and $v_{z1,2}$ $(v_{z1,i}=(\omega_{\mathbf{k}i}-\omega_c)/k_{zi})$. The main normalized parameters are $\mathbf{k}_1=(0.3,0,-0.22)$, $\mathbf{k}_2=(0.2,-0.2,-0.19)$, $\omega_{\mathbf{k}1}=0.56$, $\omega_{\mathbf{k}2}=0.53$, $v_{z1,1}=2.0$, $v_{z1,2}=2.5$, $v_{th}=5$, $\theta_{lc}=\pi/3$, and $N=10^6$.

A. Merging mechanism

As a first step, we performed numerical simulations involving two monochromatic waves interacting with a loss-cone distribution [Eq. (12)] at $n=1$ resonances, by varying p [Eq. (10)] until the dynamical resonance merging process occurred, as shown by Fig. 1 which presents the time evolution of the energy $W_{\mathbf{k}}\propto|E_{\mathbf{k}}|^2$ of two lower hybrid waves, for two different values of p. At $p=0.02$ (as well as for sufficiently small interaction intensities $p\lesssim0.02$), the two waves evolve independently [Fig. 1(a)]: for $\omega_c t/2\pi\lesssim150$, the amplitudes of both waves increase until they saturate by particle trapping around close levels; during the saturation stage $(\omega_c t/2\pi\gtrsim150)$, each of them interacts with its own population of trapped particles, showing typical oscillations around a mean energy level. At a slightly larger $p=0.025$, the waves' amplitudes are significantly increased [see Fig. 1(b), for $400\lesssim\omega_c t/2\pi\lesssim600$] and the waves' resonant widths $\delta v_{\mathbf{k}_1}$ and $\delta v_{\mathbf{k}_2}$ begin to overlap and merge. Figures 1(c) and 1(d) show the corresponding parallel velocity distributions $f_z(v_z)=\int_0^\infty 2\pi f_e(v_z,v_\perp)v_\perp dv_\perp$ at the final simulation time $\omega_c t/2\pi\simeq800$, when the merging process is fulfilled; for $p=0.02$

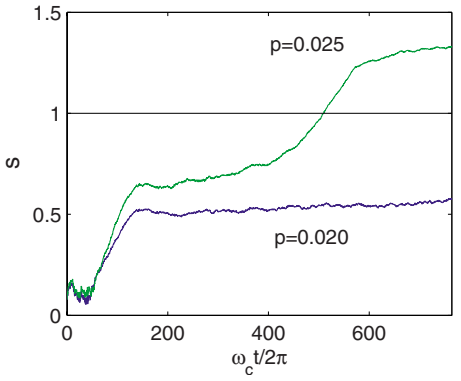

FIG. 2. (Color online) Dynamical merging of resonances: variation in the parameter s [Eq. (13)] with time, for $p=0.02$ (no merging) and $p=0.025$ (merging). The main parameters are the same as in Fig. 1.

[Fig. 1(c)], $f_z(v_z)$ is only slightly perturbed in the close vicinity of each resonant velocity $v_{z1,i}=(\omega_{\mathbf{k}i}-\omega_c)/k_{zi}$, whereas when p is increased [Fig. 1(d)], a plateau is formed in the resonance region, showing that the particles' motion is strongly perturbed. Moreover, the contour lines of the velocity distribution $f_e(v_z,v_\perp)$ at $\omega_c t/2\pi \simeq 800$ show that for $p=0.02$ [Fig. 1(e)] and $p=0.025$ [Fig. 1(f)], the resonant particles are accelerated (respectively, decelerated) along the parallel (respectively, perpendicular) direction. However, an essential difference can be observed: for $p=0.02$, two groups of particles are oscillating along the motion invariant $K=v_\perp^2/2\omega_c-v_z/k_z=cst$ [Eq. (11)], whereas for $p=0.025$, the two resonant structures have merged, i.e., some particles with velocities between the resonant velocities $v_{z1,1}$ and $v_{z1,2}$ interact strongly with the waves.

Let us introduce the dimensionless overlap parameter s as the sum of the individual resonance widths of each wave, $\delta v_{\mathbf{k}_1}$ and $\delta v_{\mathbf{k}_2}$, divided by the width $\Delta v_R=|v_{z1,1}-v_{z1,2}|$ of the resonant domain [45]

$$s=2\frac{\delta v_{\mathbf{k}_1}+\delta v_{\mathbf{k}_2}}{|v_{z1,1}-v_{z1,2}|}, \tag{13}$$

where $\delta v_{\mathbf{k}i}\simeq v_*\sqrt{(e|\varphi_{\mathbf{k}i}|_s/m_e v_*^2)|J_1(k_{\perp i}\rho_p)|_{\max}}$; ρ_p is the Larmor radius of the particle p; J_1 is the Bessel function of order 1; $|\varphi_{\mathbf{k}i}|_s$ is the potential amplitude of the wave $\mathbf{k}_i$ at saturation. Figure 2 shows that for $p=0.02$ (and thus, for $p\lesssim 0.02$), no merging occurs, s remaining approximately constant during the saturation stage, around $s\simeq 0.5$. For $p=0.025$, due to the trapping of particles, s increases up to $s\simeq 0.65$ (at $\omega_c t/2\pi\simeq 200$); then, as a result of some instability of the trapped particles, it grows slowly to reach $s\simeq 0.8$ near $\omega_c t/2\pi\simeq 400$ meanwhile the motion of the particles becomes chaotic; the consequent amplifications of the waves' amplitudes [which rise strongly between $400\lesssim\omega_c t/2\pi\lesssim 600$, see Fig. 1(b)] lead to its growth until $s\simeq 1.3$ ($\omega_c t/2\pi\gtrsim 600$), where the waves' resonant widths are largely overlapped and the merging process is fulfilled. One should note that the merging process can develop below the stochasticity threshold $s=1$, what is not expected a priori from the well-known Chirikov criterion [45,46].

B. Chaotic motion of particles

The dynamical resonance merging process, which develops when the saturation by the usual trapping mechanism is fulfilled, results from the complex dynamics of the trapped particles that oscillate in the two overlapped waves' resonance widths (or potential wells). The chaotic behavior of such particles can be pointed out by examining their trajectories. Figure 3 shows, for $p=0.025$ and three representative test particles involved in the process of merging, the variation with time of their parallel velocity v_z and their phases with respect to each of the two waves, $\zeta_{1,2}=k_{z1,2}z_p+\theta_p-\omega_{\mathbf{k}1,2}t-\arg(\varphi_{\mathbf{k}1,2})$ (θ_p is the azimuthal angle of the particle). As shown by Figs. 3(a) and 3(b), during the stage of saturation by trapping ($\omega_c t/2\pi\lesssim 400$), the particles may be alternatively trapped by one wave or by the other, keeping a quite constant phase relation with it, i.e., $d\zeta_{1,2}/dt<k_{z1,2}(e|\varphi_{\mathbf{k}1,2}|/m_e)^{1/2}$, and undergoing fast oscillations due to the perturbation of their motion by the other wave. Figure 3(c) presents an example where the particle is not trapped by any wave for $\omega_c t/2\pi\lesssim 400$; its phase relatively to each wave evolves monotonically. After the merging of the two resonant domains ($\omega_c t/2\pi\gtrsim 600$), the particles can be alternatively trapped by one wave, by the other one or by both simultaneously, performing in the latter case oscillations over the overlapped velocity region. Anyway, as the particles are, during their motion, performing a large number of stochastic transitions between the states where they are trapped or passing [39], it is reasonable, in order to derive analytical estimates of the waves' amplitudes and the relaxed electron distributions, to assume that the motion of the particles in the overlapped waves' potential region is randomlike (see next paragraph).

C. Asymptotic stage of the wave-particle system

As the merging process is fulfilled when the waves' resonance widths have overlapped, it is possible, assuming that the particles' motion is randomlike in the overlapped domain of width Δv_{RM}, to estimate the energy gained by the waves during the process by using the conservation of the momentum [Eq. (2)]. Let us assume that Δv_{RM} is approximately equal to the width $\Delta v_R=|v_{z1,1}-v_{z1,2}|$ between the two resonant velocities (as shown by the numerical simulations) and much larger than the resonant widths $\delta v_{\mathbf{k}i}$ of each individual wave at the saturation stage of the linear instability, that is

$$\Delta v_{RM}\simeq|v_{z1,1}-v_{z1,2}|\gg\frac{\gamma_{\mathbf{k}1,2}}{k_{z1,2}},\quad\left(\frac{e|\varphi_{\mathbf{k}1,2}|_s}{m_e}\right)^{1/2}, \tag{14}$$

where $\gamma_{\mathbf{k}1,2}$ are the linear growth rates of the waves. One can observe that, because $\Delta v_{RM}\gg\gamma_{\mathbf{k}1,2}/k_{z1,2}$, the variation δP_m of the momentum after the merging has occurred strongly exceeds its variation δP_s after the individual saturation of the waves by trapping is achieved: $\delta P_m\gg\delta P_s$. Then, on the basis of the wave-particle momentum balance [Eq. (2)], one can deduce that the waves' amplitudes are several times larger at the asymptotic stage of the merging process than at the time when the saturation due to trapping by individual waves is reached.

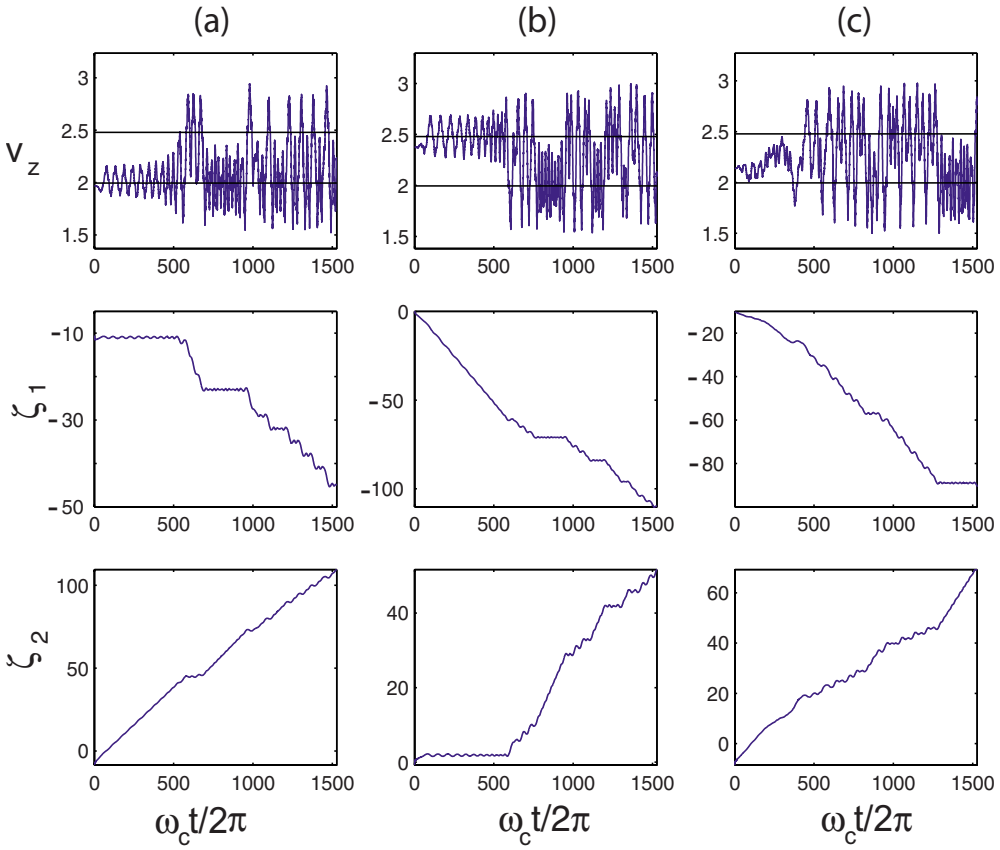

FIG. 3. (Color online) Trajectories of three test particles (a)–(c) oscillating in the overlapped potential wells of two waves. The upper row shows the variation in the parallel velocity v_z of the test particles as a function of $\omega_c t/2\pi$; the horizontal lines represent the unperturbed cyclotron resonant velocities of the waves, $v_{z1,1}$ and $v_{z2,2}$. The middle and lower rows show the variation in the particle phases relatively to each wave, $\zeta_{1,2}=k_{z1,2}z_p+\theta_p-\omega_{\mathbf{k}1,2}t-\arg(\varphi_{\mathbf{k}1,2})$. The main parameters are the same as in Fig. 1, with $p=0.025$.

If the waves' resonance widths are not overlapping and Eq. (14) is valid, each wave interacts with its own resonant group of particles so that the saturation levels reached by the waves result from usual trapping processes [see Fig. 1(a)]. In the opposite case, when the resonance widths are overlapping, i.e., when Eq. (14) is no more valid, the particles interact with the two waves simultaneously, and their motion becomes stochastic: the merging process takes place, leading to a significant increase in the waves' amplitudes [see Fig. 1(b), $\omega_c t/2\pi \gtrsim 400$]. This mechanism results from the complex dynamics of the resonant particles moving in the field of one wave under the perturbation of the other one and can be considered in a first approximation as a parametric instability with a threshold depending on the wave-particle interaction parameter p and with a frequency modulation proportional to the ratio of the waves' amplitudes reached at saturation by trapping [36]. The threshold is defined by Eq. (14), but its exact expression as a function of p and the other characteristic parameters (as ω_p/ω_c, θ_{lc},…) has not been determined yet.

Figure 4 shows the relaxed distribution $f_e(v_z,v_\perp)$ after its interaction with the two waves (i) when no dynamical resonance merging occurs [Fig. 4(a)] and (ii) when the process takes place [Fig. 4(b)]. It clearly shows that in the first case, the two waves behave independently, each of them trapping electrons with velocities v_z close to its resonant velocity. The structure of the relaxed distribution is then the superposition of the two perturbations due to a single wave, the particles moving along the invariant line $K=m_e(v_\perp^2/2\omega_c-v_z/k_z)=cst$. On the contrary, when the merging process takes place, the two structures merge in a larger one of similar shape [Fig. 4(b)]. The process generates a large amplification of the waves' energies [see also Fig. 1(b)] which finally saturate due to phase mixing of particles in the domain Δv_{RM}.

IV. SATURATION AND RELAXATION PROCESSES

Numerical simulations involving dense wave spectra with different initial distributions in **k** space have been performed, meanwhile various types of particle distributions presenting loss-cone structures have been considered: (i) the so-called single-sided loss-cone $f_{slc}(v_z,v_\perp)$ (see, e.g., Fig. 10, upper left panel), (ii) the double-sided loss-cone $f_{dlc}(v_z,v_\perp)$ (see, e.g., Fig. 10, middle left panel) and (iii) the Maxwellian with loss-cone $f_{mlc}(v_z,v_\perp)$ (see, e.g., Fig. 10, bottom left panel). Such kinds of distributions and combinations thereof are close to those observed in space and laboratory plasmas; however, in spite of the fact that loss-cone structures are usually the result of some physical processes, they can also be used as initial distributions, in order to study the further evolution of wave-particle systems. Moreover, the three types of loss-cone distributions studied hereafter are suitable

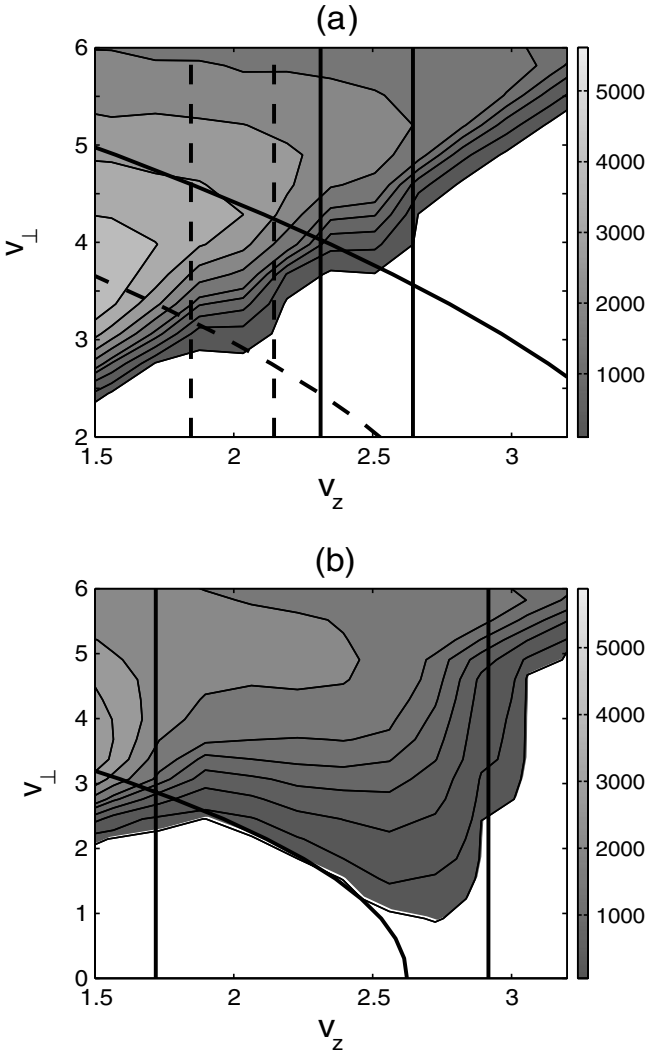

FIG. 4. Relaxation stage of the particle distribution $f_e(v_z, v_\perp)$. (a) No dynamical resonance merging occurs ($p=0.02$); the vertical lines represent the maximum velocity accessible to the particles trapped in the two waves' potentials [dashed (respectively, solid) lines for the first (respectively, second) wave]; the curves show correspondingly, for each wave, the minimum value of the motion invariant $K=m_e(v_\perp^2/2\omega_c - v_z/k_z)=cst$. (b) The dynamical resonance merging process occurs ($p=0.025$); the vertical lines show the boundaries of the overlapped domain of width Δv_{RM}, whereas the curve represents the minimum value of the invariant K for the particles moving within Δv_{RM}. The main parameters are the same as in Fig. 1.

for numerical modeling and allow us to provide a rather simple description of the physical results obtained.

A. Waves' and particles' nonlinear dynamics

Let us first discuss the case of a single-sided loss-cone distribution $f_{slc}(v_z, v_\perp)$, with $v_z > 0$ for all particles. Thus, only waves propagating with $k_z < 0$ can interact with them at normal cyclotron resonance velocities $v_{zn}=(\omega_{\mathbf{k}} - n\omega_c)/k_z > 0$, $n \geq 1$. Note that the distribution of the wave vectors in the perpendicular plane is chosen quite isotropic and most of the waves verify $|k_z/k_\perp| < 1$ and $\omega_{\mathbf{k}}/\omega_c < 1$, correspondingly. The variation with time of the waves' and particles' energy densities is presented in Figs. 5(d)–5(f). The first saturation stage of the wave amplitudes' growth, due to particle trapping, is followed by a sharper increase resulting from the dynamical resonance merging process ($200 \lesssim \omega_c t/2\pi \lesssim 600$): Fig. 5(d) shows the strong growth of the total wave energy density $W=\Sigma_{\mathbf{k}} W_{\mathbf{k}}$, which saturates near $\omega_c t/2\pi \simeq 900$ and then decreases to some lower level, in agreement with the variation in the total particle kinetic energy $\mathcal{E} \propto n_{res}\langle v^2\rangle/2$ for $\omega_c t/2\pi \gtrsim 900$ [Fig. 5(f)]. During the wave-particle interactions, the perpendicular (respectively, parallel) kinetic energy density $\mathcal{E}_\perp \propto n_{res}\langle v_\perp^2\rangle/2$ (respectively, $\mathcal{E}_z \propto n_{res}\langle v_z^2\rangle/2$) is decreasing (respectively, increasing), indicating that particles are accelerated along the magnetic field, whereas they loose energy during their perpendicular motion [Fig. 5(f)]. The time variation in the energy densities $W_{\mathbf{k}}$ of the waves with the largest saturation amplitudes is shown in Fig. 5(e). The particle distribution $f_{slc}(v_z, v_\perp)$ is presented at the initial time [Fig. 5(a)], during the merging process [Fig. 5(b)] and after its completion, when the loss cone is filled with particles [Fig. 5(c)]. Note that, after the wave energy W has reached its maximum near $\omega_c t/2\pi \simeq 900$, it starts to decrease because, owing to the partial filling of the loss-cone at this stage, the instability growth rates change sign for a part of the waves (those which reached first the saturation). Nevertheless, this does not stop the filling of the cone and a near equilibrium particle distribution is established, whose energy exchanges with most waves vanish. However, a full balance is not yet realized: the wave spectrum and the particle distribution continue to slowly evolve. Indeed, some of the waves do not stop to grow whereas others damp; the particles which fill the cone loose perpendicular kinetic energy ($\Delta\mathcal{E}_\perp < 0$) but gain parallel one ($\Delta\mathcal{E}_z > 0$); the total kinetic energy $\mathcal{E}$ starts to increase slowly, whereas W is reduced correspondingly [see Figs. 5(d) and 5(f)]. As shown below, the existence of interactions at Landau ($n=0$) or anomalous cyclotron ($n \leq -1$) resonances modifies the dynamics of the waves. Therefore, in the case when only normal cyclotron resonances $n \geq 1$ are considered, we do not study the further waves' evolution as well as the question whether a full balance can be reached and what energy is finally carried by the waves.

Particles' trajectories have also been examined and their behavior is qualitatively very close to that described in the previous section as well as in the case of the fan instability at $n \leq -1$ [36,37]. Typically, the particles' dynamics is stochastic and cannot be described in its totality by a classical diffusion as in the frame of the quasilinear theory nor by usual trapping processes at work in the presence of several wave troughs. The particles oscillate in the potential well formed by a subset of the most intense waves which are able to trap them, jumping from the potential well formed by a subset of waves to another one.

B. Influence of the wave spectrum characteristics on the merging and the saturation processes

Figure 6 shows the time variation in the total wave energy density W calculated for three different wave packets inter-

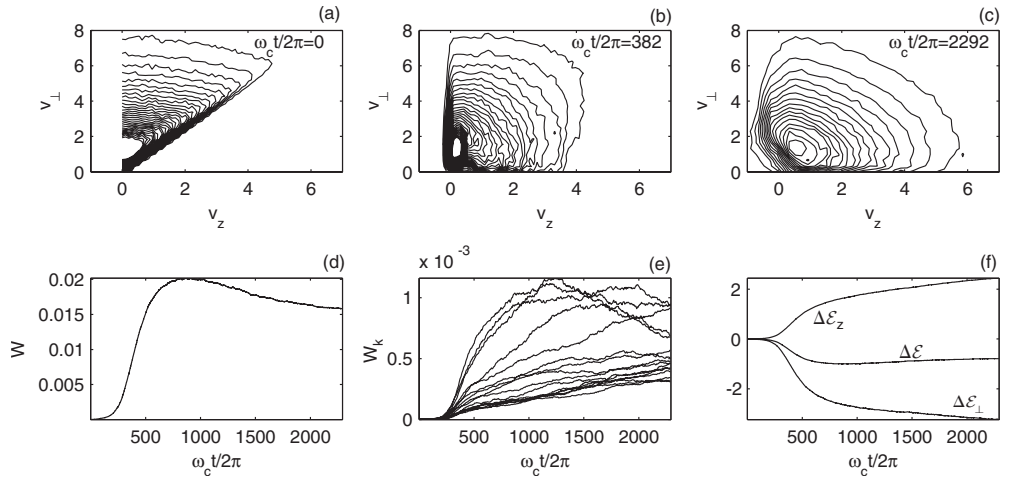

FIG. 5. Evolution of the waves and particles interacting at normal cyclotron resonances $n \geq 1$. Particle distribution $f_{slc}(v_z, v_\perp)$ at (a) the initial time, (b) during the dynamical merging process and (c) at the asymptotic stage. (d) Time evolution of the total wave energy density W. (e) Time evolution of the energy densities $W_{\mathbf{k}}$ of the waves with the largest saturation amplitudes. (f) Variation in the parallel, the perpendicular, and the total kinetic energies, $\Delta\mathcal{E}_z$, $\Delta\mathcal{E}_\perp$, and $\Delta\mathcal{E}$, respectively. The main parameters are: $\omega_p/\omega_c=1$, $p=0.02$, $N_w=200$, and $N=500\,000$.

acting with the same particle distribution; they contain $N_w=100$, 200, and 300 waves, respectively, and present different distributions in **k** space. In spite of the noticeable differences between the energy spectra of the three wave packets (see Fig. 7)—and thus between the time histories of their relaxation processes—their energy densities W reach close levels at saturation. Moreover, the final relaxed particle distributions are very similar too (not shown here). This result indicates that, if the waves are distributed in **k** space rather continuously (i.e., without large gaps between their resonant velocities), the initial wave-packet distribution does not influence essentially on the system's evolution. Moreover, relevant numerical calculations indicate that, if the main parameters as the particle velocity distribution along z, $f_z(v_z)=\int_0^\infty f_e(v_z,v_\perp)d(\pi v_\perp^2)$, and the total width Δv_R of the resonant velocities are fixed, the general features of the relaxed particle flux and of the waves' energy evolution weakly depend on the waves' distribution. Figure 7 shows the energy spectra of the wave packets corresponding to Fig. 6, i.e., the energy density of the waves, $W_{\mathbf{k}}$, versus their resonant velocities $v_{z1}=(\omega_{\mathbf{k}}-\omega_c)/k_z$ $(n=1)$, at different times during the merging process $(200 \lesssim \omega_c t/2\pi \lesssim 800)$ and in the asymptotic saturation stage $(800 \lesssim \omega_c t/2\pi \lesssim 1035)$. One observes that the dynamical resonance merging depends on the number of waves N_w and occurs with different rates for various domains of the resonant velocities v_{z1}. As result, a few perturbations appear in the particle distribution at intermediate times (not shown here); in the further evolution they merge in a com-

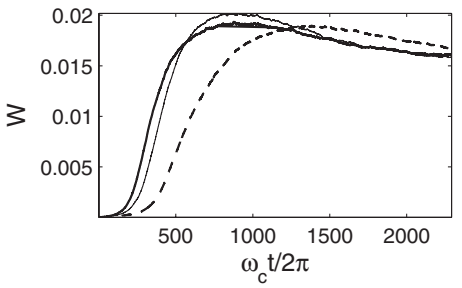

FIG. 6. Time evolution of the total wave energy density W for three different waves' distributions in **k** space, corresponding to $N_w=100$ (dashed curve), $N_w=200$ (thin solid curve), and $N_w=300$ (thick solid curve). The waves interact at normal cyclotron resonances $n \geq 1$ with the same particle distribution. The main parameters are: $\omega_p/\omega_c=1$, $p=0.02$, and $N=500\,000$.

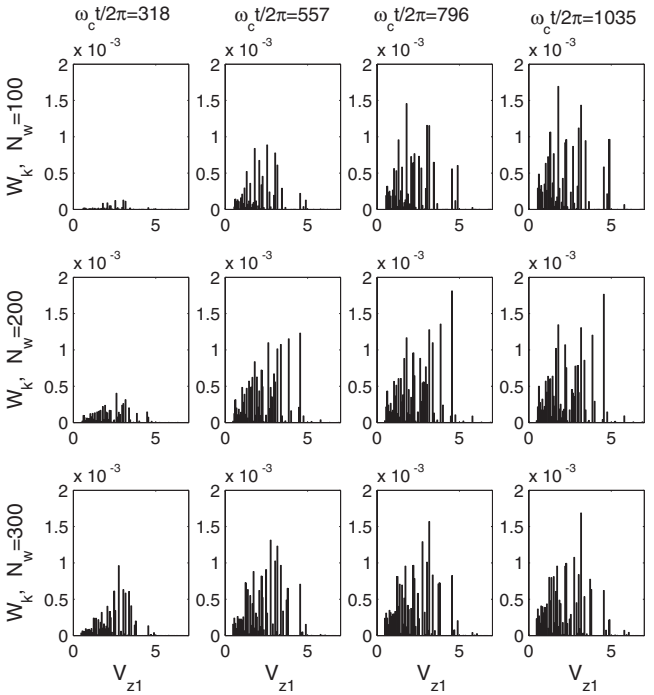

FIG. 7. Time evolution of the three wave packets of Fig. 6: energy density of the waves, $W_{\mathbf{k}}$, as a function of the normal cyclotron resonant velocities $v_{z1}=(\omega_{\mathbf{k}}-\omega_c)/k_z$, at four different times. Top row: $N_w=100$; middle row: $N_w=200$; bottom row: $N_w=300$. The parameters are the same as in Fig. 6.

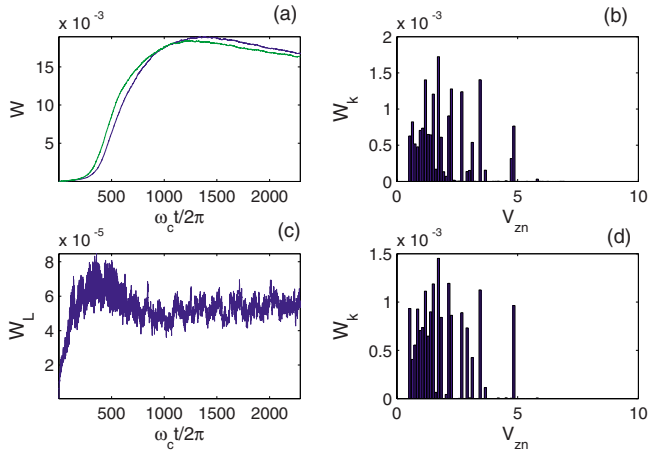

FIG. 8. (Color online) (a) Variation in W with time, showing two curves: when the waves interacting at Landau resonances are (i) present and (ii) not present; (c) time evolution of the energy density W_L of the Landau resonant waves; [(b) and (d)] energy densities of the waves, $W_{\mathbf{k}}$, as a function of their resonant velocities v_{zn}, for the final simulation time, when the Landau resonant waves are present or not [respectively, (d) and (b)]. A single-sided loss-cone distribution is considered. The main parameters are: $\omega_p/\omega_c=1$, $p=0.02$, $N=500\,000$; for (a)–(i): $N_w=200$ (respectively, 100) waves with $k_z<0$ (respectively, $k_z>0$) are interacting at normal cyclotron (respectively, Landau) resonances; for (a)–(ii): $N_w=100$ waves with $k_z<0$ are interacting at normal cyclotron resonances.

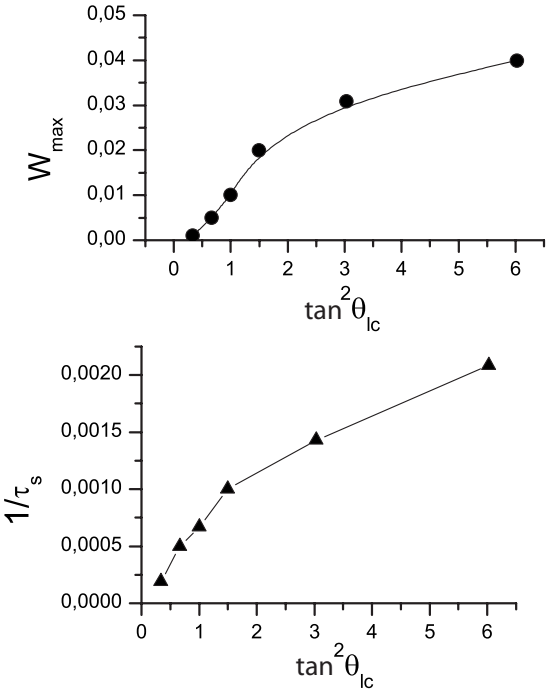

FIG. 9. Variation as a function of $\tan^2\theta_{lc}$ of the wave energy density at saturation, $W_{\max}$, and of the inverse of the time τ_s when it is reached. Single-sided loss-cone distributions are considered. The main parameters are $\omega_p/\omega_c=1$, $p=0.02$, $N=500\,000$, and $N_w=200$.

mon structure which fills the empty loss-cone [see also Fig. 5(c)].

C. Role of the Landau damping

The numerical calculations show that the role of the Landau resonances $n=0$ (waves with $k_z>0$) in the evolution of a single-sided loss-cone distribution $f_{slc}(v_z,v_\perp)$ is not essential, because $\partial f_{slc}/\partial v_z<0$ in the considered region $v_z>0$ where the particles are located, so that no bump-on-tail instability can develop. However, that is not true near $v_z\simeq 0$, but this domain is out of our scope because, according to our model, it is occupied by the bulk formed by the nonresonant electrons. So, all waves interacting at $n=0$ are supposed to be strongly damped. The small role of the Landau damping is illustrated by Fig. 8(a) which shows the variation in W as a function of time, when the Landau resonant waves are present or not: the two curves are almost indistinguishable. The time evolution of the energy density W_L of the Landau resonant waves is presented in Fig. 8(c), which shows their negligible contribution, as $W_L/W\ll 1$. The wave energy spectra, i.e., the variation in $W_{\mathbf{k}}$ with the resonant velocities v_{zn}, are shown for the final simulation time, when the Landau resonant waves are present [Fig. 8(d)] or not [Fig. 8(b)].

D. Loss-cone filling by particles

Moreover, simulations have also been performed for different values of the loss-cone angle θ_{lc} [Eq. (12)], keeping the same plasma parameters and wave packet. Figure 9 presents the variations with $\tan^2\theta_{lc}$ of the wave energy density at saturation, $W_{\max}$, and the time τ_s when it is reached. Examining the corresponding distributions $f_e(v_z,v_\perp)$ shows that for $\omega_c t/2\pi\geq\tau_s$, the loss-cone is almost filled so that τ_s can be considered as a good estimate of the filling time. One could expect that $\tau_s^{-1}\sim\gamma_{\max}$ (where $\gamma_{\max}$ is the maximum growth rate of the waves), but this is not proved by the simulations. However, at small θ_{lc} one can explain the observed dependence of $W_{\max}$ using the balance of energy

$$W_{\max}=\sum_{\mathbf{k}}\mathbf{k}^2|\varphi_{\mathbf{k}}|_s^2\propto\left|\delta\left(\int v^2 f_e(v,\theta)d\mathbf{v}\right)\right|, \qquad (15)$$

where $d\mathbf{v}=2\pi v^2 dv d(\sin\theta)$. First, note that during the wave-particle interactions, kinetic energy is exchanged between the parallel direction and the perpendicular plane, whereas the variation $\Delta\mathcal{E}$ of the total kinetic energy is essentially smaller so that the isotropization of the velocity distribution $f_e(v_z,v_\perp)$ occurs. Second, for small θ_{lc}, one can assume that in the area out of the cone, $f_e(v_z,v_\perp)$ slightly varies; indeed, it is only reduced by a factor $(1+\sin\theta_{lc})^{-1}$, i.e., it changes its normalization, which corresponds to the increase in the phase-space volume in which the total number of particles is distributed after the cone is filled. Then, the integral variation in Eq. (15) is caused by the reduction in the number of particles out of the cone and by the changes occurring in the cone area after its filling. It is natural to assume that inside or outside the cone, the distributions $f_e(v_z,v_\perp)$ do not differ. Then, the integral variation

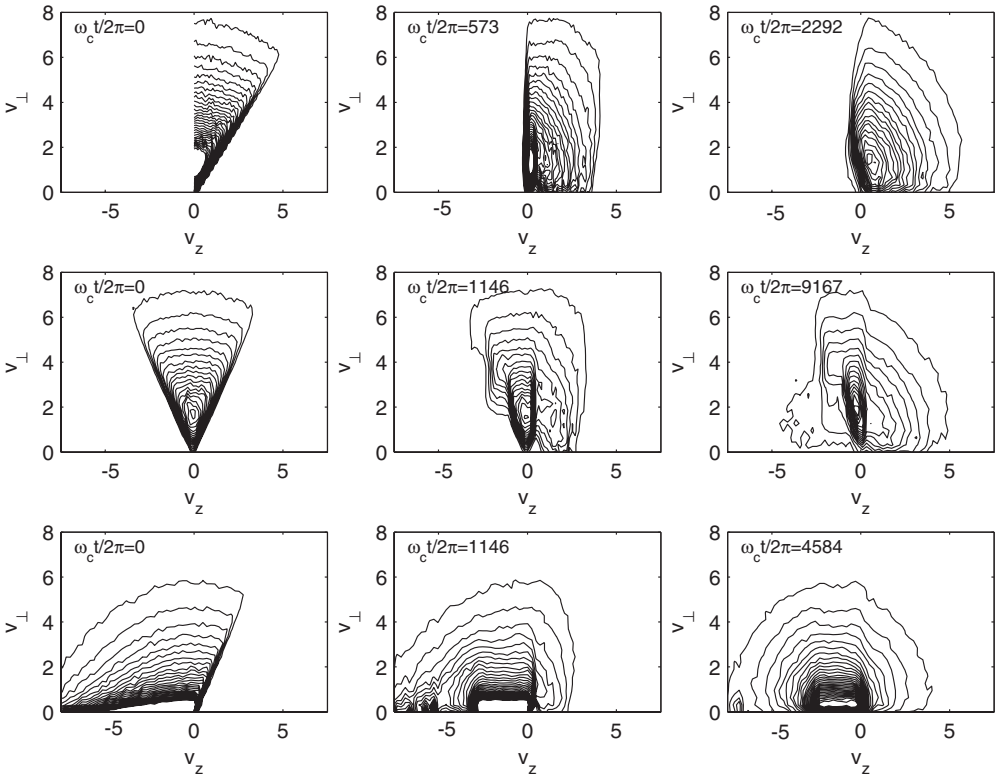

FIG. 10. Particle velocity distributions $f_e(v_z, v_\perp)$ at three moments of time. Top, middle and bottom rows correspond, respectively, to a single-sided loss-cone ($f_e=f_{slc}$), a double-sided loss-cone ($f_e=f_{dlc}$), and a Maxwellian with loss-cone ($f_e=f_{mlc}$) distribution. The wave spectrum is asymmetric ($k_z<0$ for all waves). The main parameters are: $\omega_p/\omega_c=1$, $p=0.02$, $N=500\,000$, and $N_w=100$.

$$\left|\delta\left(\int v^2 f_e(v,\theta)d\mathbf{v}\right)\right| \propto \left|\int_{\theta_{lc}}^{\pi/2}\left(1-\frac{1}{1+\sin\theta_{lc}}\right)d(\sin\theta) - \int_0^{\theta_{lc}}\frac{d(\sin\theta)}{1+\sin\theta_{lc}}\right| \sim \sin^2\theta_{lc} \simeq \theta_{lc}^2 \tag{16}$$

appears to be proportional to θ_{lc}^2, in good agreement with the results presented in Fig. 9(a) for $\theta_{lc} \ll 1$, revealing that $W_{\max} \propto \tan^2\theta_{lc}$. Moreover, for small θ_{lc}, Fig. 9(b) shows that $1/\tau_s \propto \theta_{lc}^2$ so that the filling time τ_s decreases when θ_{lc} increases. For large θ_{lc}, the made above assumptions are broken, and it is not possible to use simple arguments to explain the results of Fig. 9, which show that $W_{\max}$ grows slowly with θ_{lc}.

E. Influence of the particle distribution on the system's dynamics

As mentioned above, for $f_e=f_{slc}$, when all resonant particles have positive velocities $v_z>0$, their interactions with the waves at $n=0$ do not influence noticeably on the dynamics of the system during the instability development. But when particles with $v_z<0$ are present, the role of the resonances $n=0$ rises, in agreement with simulations performed for double-sided loss-cone f_{dlc} and Maxwellian with loss-cone f_{mlc} distributions. Indeed, Fig. 10 shows for comparison the time evolution of three kinds of initial distributions involving a loss-cone, for the same wave packet, which is anisotropic in $\mathbf{k}$ space and whose waves verify $k_z<0$. In the first case (Fig. 10, top row, $f_e=f_{slc}$), no (respectively, all) particles interact at $n=0$ (respectively, $n\geq 1$) with the waves; in the second case (Fig. 10, middle row, $f_e=f_{dlc}$), the unstable waves which interact at $n\geq 1$ with particles of velocities $2\lesssim v_z\lesssim 6$ also interact at $n=0$ with particles in the range $-3\lesssim v_z\lesssim -1$. In the third case (Fig. 10, bottom row, $f_e=f_{mlc}$), a part of the waves interact at $n\leq -1$ with particles of velocities $v_z\lesssim -3$; the share of particles getting to such resonances is essentially larger than in the second case.

For the three cases presented in Fig. 10, the evolution of $f_e(v_z, v_\perp)$ in the region $v_z>0$ is similar and the cone is finally filled. But unlike the case when $f_e=f_{slc}$ (top row), the second distribution $f_e=f_{dlc}$ reveals the formation of a particle "tail" extending along $-\mathbf{B}_0$ (middle row, right panel). It results from the interaction of particles with Landau resonant waves, but not only; indeed, some analysis [36] (not presented here) shows that if the density of the particles interacting with waves at $v_{zn}=(\omega_{\mathbf{k}}-n\omega_c)/k_z$ ($n\geq 1$) is large (i.e., $p\gtrsim 0.02$) and, accordingly, if the wave amplitudes are high enough, it is necessary to take into account the resonant interaction of particles with the beatings of some waves. The stabilizing influence of the particles with $v_z<0$ leads to the reduction in the total growth rate of the loss-cone instability, for f_{dlc} in comparison with f_{slc}, and to the reduction in $W_{\max}$ due to the acceleration of particles with $v_z<0$. This is illustrated by Fig. 11 which shows the time variation in W for the three distributions considered in Fig. 10: the curves (1), (2), and (3) correspond, respectively, to $f_e=f_{slc}$, $f_e=f_{mlc}$, and f_e

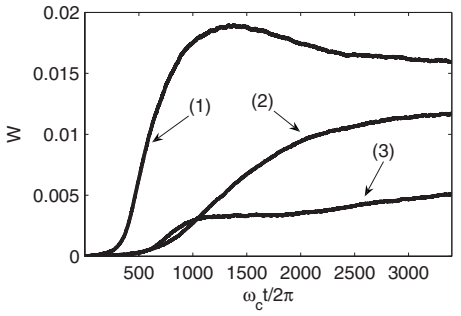

FIG. 11. Variation in W with time. The curves (1), (2), and (3) correspond, respectively, to $f_e=f_{slc}$, $f_e=f_{mlc}$, and $f_e=f_{dlc}$. The wave spectrum is asymmetric ($k_z<0$ for all waves). The main parameters are the same as in Fig. 10.

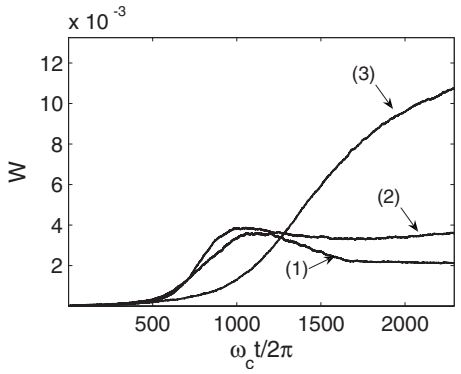

FIG. 12. Variation in W with time. The curves are labeled as follows: (1) $f_e=f_{dlc}$, with an asymmetric wave spectrum, (2) $f_e=f_{dlc}$, with a symmetric spectrum, and (3) $f_e=f_{mlc}$, with a symmetric spectrum. The three distributions have the same loss-cone angle θ_{lc}. The main parameters are: $\omega_p/\omega_c=1$, $p=0.02$, $\theta_{lc}=60°$, $N=500\,000$; $N_w=100$ (respectively, $N_w=200$) for the asymmetric (respectively, symmetric) wave spectrum.

$=f_{dlc}$. Note that for the curve (3) (see also the middle row of Fig. 10) the particle density in the region of the loss-cone is twice less than for the curve (1) (see also the top row of Fig. 10); however, this cannot explain the different energy levels reached at saturation. In particular, the curve (2) essentially differs from the two other ones; although one can expect a stronger stabilizing effect due to the particles with $v_z<0$, the wave energy grows to a higher level than for the case of a bilateral cone of losses [curve (3)]; moreover, the kinetic energies $\mathcal{E}_z$ and $\mathcal{E}_\perp$ are reduced and no exchanges between them is observed, as it is for the cases (1) and (3). This feature will be considered in more details below (Figs. 14 and 15).

F. Competition between the resonances

1. Landau and normal cyclotron resonances

Let us now consider the role of the $n=0$ and $n\leq -1$ resonances on the system's evolution for distributions f_e involving particles at $v_z<0$. Above we considered a double-sided loss-cone distribution $f_{dlc}(v_z,v_\perp)$ interacting with an asymmetric spectrum of waves with $k_z<0$ (Fig. 10). Let us compare these results with the case of a symmetric spectrum containing also waves with $k_z>0$, all of them being distributed rather regularly. Figure 12 presents the corresponding variation in W with time for three different distributions f_e with the same loss-cone angle θ_{lc}: the difference between the results obtained using a double-sided loss-cone with a symmetric [curve (1)] and an asymmetric [curve (2)] wave spectrum is not significant and consists mainly in a more or less small decrease in W in the saturation stage; for the curve (3) with $f_e=f_{mlc}$, W reaches a higher value than in both other cases. Figure 13 shows three moments of the time evolution for the distributions considered in Fig. 12. One can see that, for an asymmetric wave spectrum, the process of cone filling develops asymmetrically (top row); thus, as already marked above (Fig. 10), the appearance of particles inside the cone at $v_z<0$ results from their interactions with waves at $n=0$ and with the beatings of some waves. The latter effect depends nonlinearly on the waves' amplitudes [36], it weakens or almost disappears when the number of resonant particles is reduced whereas the wave amplitudes accordingly decrease. The filling of the cone in the case of symmetric wave spectra occurs symmetrically (Fig. 13, middle row); the asymmetries appearing at intermediate stages of the evolution are connected with the different values of the waves' growth rates, which depend on the initial conditions. In the case of a symmetric spectrum and a Maxwellian with loss-cone distribution f_{mlc} (Fig. 13, bottom row), not only filling of the cone occurs but also some essential deformation of the distribution at $v_z<0$, in the region where it is supposed that the interactions of waves with particles lead to their attenuation, i.e., where the particles get energy from the waves. However, it appears that it is not so.

2. Role of the anomalous cyclotron resonances

As we explain below, Fig. 14 presents the evolution of the three considered distributions as a function of v_z, i.e., $f_z(v_z)=\int_0^\infty 2\pi v_\perp f_e(v_z,v_\perp)dv_\perp$, for two moments of time. For a symmetric wave spectrum, some particles interact at $n\geq 1$ resonances with waves, causing their instability. The same waves get to Landau resonances $n=0$ with particles of small velocities (i.e., $|v_z|\lesssim 2.5$ for Fig. 13); however, if conditions of loss-cone instability are realized, these particles do not stabilize the growth of the waves but produce some flattening in the region where $|v_z|\lesssim 2.5$ (Fig. 14, middle row). After the wave amplitudes grow up to noticeable levels, these particles start to get energy from (or to give to) the waves and their parallel velocities vary within the range of the Landau resonance velocities $v_{z0}=\omega_{\mathbf{k}}/k_z$. For an asymmetric spectrum, note the formation of an appreciable plateau for $-2.5\lesssim v_z\lesssim -1$ at $\omega_c t/2\pi=8021$ (Fig. 14, top row), which results from the interaction of particles with waves at $n=0$ resonances; the further appearance of a tail (Fig. 13, top row) is most likely connected with the acceleration of particles under the influence of wave beatings, as direct resonant wave-particle interactions are absent in this velocity range.

In the case of a Maxwellian with loss-cone distribution, the situation is more complicated, because interactions at $n\leq -1$ resonances become essential too. Note that such effect is not significant for the above considered cases with double-

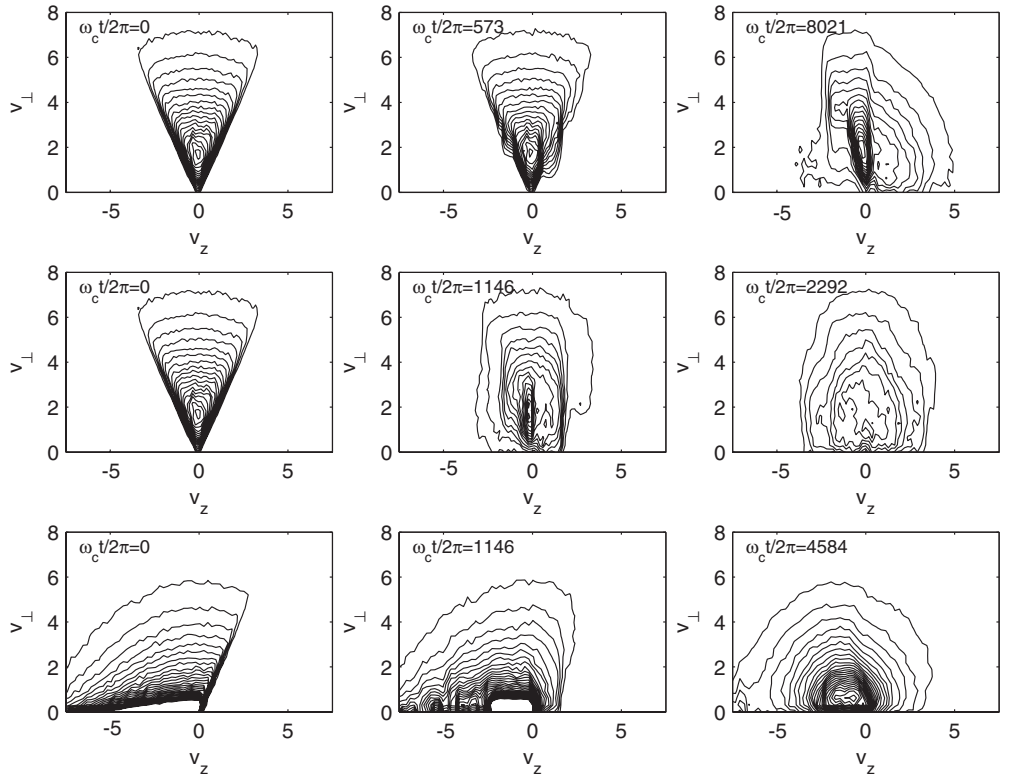

FIG. 13. Particle velocity distributions $f_e(v_z, v_\perp)$ at three moments of time. Top, middle, and bottom rows correspond, respectively, to the distributions (1), (2), and (3) of Fig. 12. The main parameters are the same as in Fig. 12.

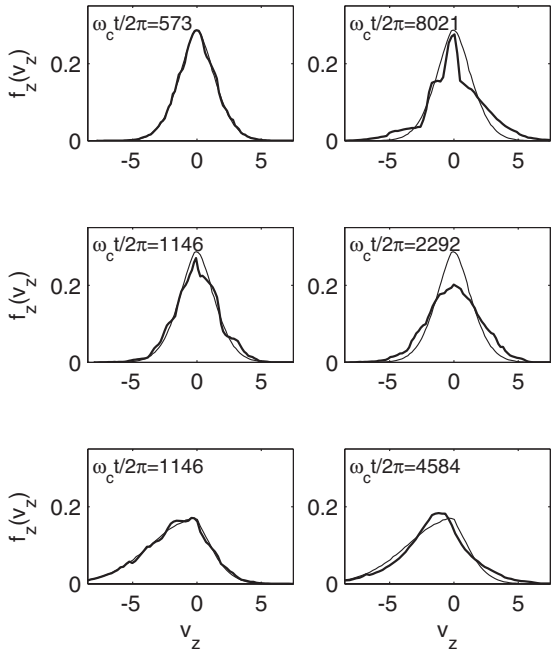

FIG. 14. Parallel velocity distributions $f_z(v_z) = \int_0^\infty 2\pi v_\perp f_e(v_z, v_\perp) dv_\perp$ at two moments of time (thick solid lines); the initial distributions are represented by thin solid lines. Top, middle, and bottom rows correspond, respectively, to the distributions (1), (2), and (3) of Fig. 12. The main parameters are the same as in Fig. 12.

and single-sided loss-cone distributions when only few particles interact at $n \leq -1$ with the waves. To this resonant effect is superposed a process of plateau formation, which occurs at small velocities and is well appreciable (Fig. 14, bottom row). As a result of these two factors, the conditions for wave stabilization change and some instability of the fan type can develop, if $f_z(v_z)$ is anisotropic and interactions at $n \leq -1$ prevail [35,37,38] (note that, because waves with finite amplitudes are considered, it would be more proper to speak here of resonant interactions of waves with particles and not of linear instability). The waves with $k_z < 0$ gain some energy due to their interactions at $n \leq -1$ with particles of velocities $v_z < 0$, which loose parallel kinetic energy $\mathcal{E}_z$, that is partly transferred to the perpendicular motion and to the waves. This process manifests itself by an appreciable reduction in $f_z(v_z)$ for $-7 \lesssim v_z \lesssim -2.5$ (see Fig. 14, bottom row, right panel). Thus, unlike the distributions f_{slc} and f_{dlc}, not only $\mathcal{E}_\perp$ but also $\mathcal{E}_z$ decreases. This effect is more visible for a widely open loss-cone distribution (see Fig. 15, left panel, $\theta_{lc}=67.6°$). After the formation of a plateau in the region of the Landau resonant velocities v_{z0}, only interactions at $n \geq 1$ (for $v_z > 0$) and at $n \leq -1$ (for $v_z \lesssim -2$) start to compete; at the same time, in both cases the waves gain on average energy from the particles. But for $\theta_{lc}=45°$, by scattering on the waves, $\mathcal{E}_\perp$ decreases whereas $\mathcal{E}_z$ increases (Fig. 15, right panel); for $\theta_{lc}=67.6°$ (Fig. 15, left panel), the exchanges of kinetic energy between the parallel direction and the perpendicular plane work in another way, as the total energy balance depends on the relative number of particles involved in each kind of resonant interaction. When θ_{lc} in-

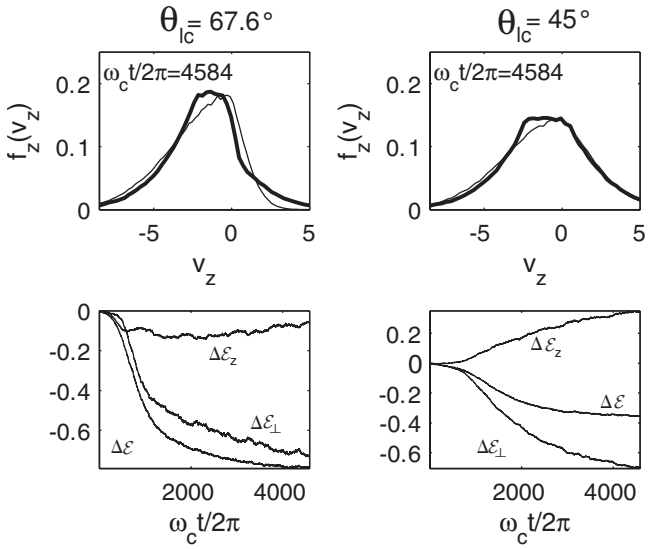

FIG. 15. For two Maxwellian with loss-cone distributions, with $\theta_{lc} \simeq 67.6°$ (left panels) and $\theta_{lc} \simeq 45°$ (right panels): Top row: initial (thin line) and final (thick line) parallel velocity distribution $f_z(v_z)$; bottom row: variation with time of the total, the perpendicular and the parallel kinetic energies, $\Delta\mathcal{E}$, $\Delta\mathcal{E}_\perp$, and $\Delta\mathcal{E}_z$, respectively. The main parameters are: $\omega_p/\omega_c=1$, $p=0.02$, $N=500\,000$, and $N_w=200$.

creases, the relative number of particles involved in interactions at $n \geq 1$ decreases, what explains the sign inversion in the variation in $\mathcal{E}_z$ when passing from $\theta_{lc}=45°$ to $\theta_{lc}=67.6°$ (compare right and left panels of Fig. 15, bottom row).

To support this picture we present in Fig. 16 the variation with time of the parallel velocity v_z of three typical test particles. The resonant velocities $v_{zn}=(\omega_{\mathbf{k}}-n\omega_c)/k_z$ for $n=\pm 1$ and $n=0$ are represented by horizontal lines. One observes that each particle interacts strongly with the waves: the first

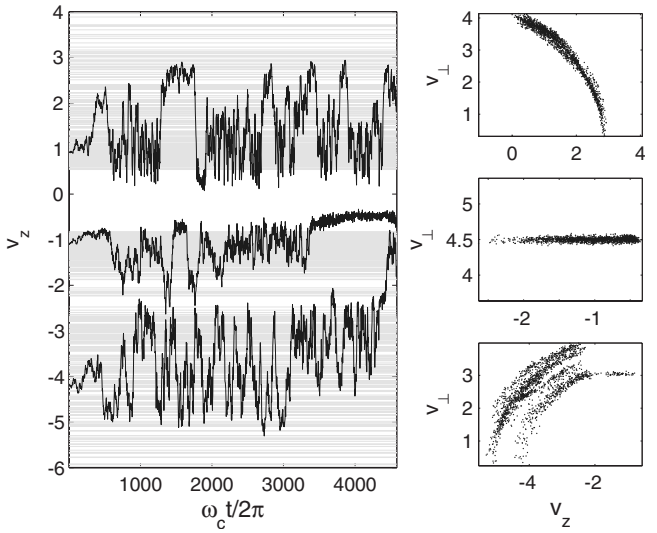

FIG. 16. Trajectories of three test particles. Left panel: variation in v_z with time; the horizontal lines represent the resonant velocities ($n=0$ and $n=\pm 1$ resonances are considered). Right panels: corresponding trajectories in the $(v_z, v_\perp)$ plane. The main parameters are $\omega_p/\omega_c=1$, $p=0.02$, $N=500\,000$, and $N_w=200$.

one oscillates mainly around the normal cyclotron resonant velocities v_{z1}, with $0 \lesssim v_z \lesssim 3$; the second (respectively, third) one, with $-2.5 \lesssim v_z \lesssim -0.3$ (respectively, $-5.5 \lesssim v_z \lesssim -1$), interacts mainly at $n=0$ (respectively, $n=-1$) with the waves. Each particle is successively trapped by different subsets of waves, according to the complex process of multitrapping [37]. In particular, the third one is trapped by waves at $n=-1$ (respectively, $n=0$), for $\omega_c t/2\pi \lesssim 4300$ (respectively, $\omega_c t/2\pi \gtrsim 4300$); after Landau resonant interactions, the second particle is no more trapped by any wave and is freely accelerating in the range $3300 \lesssim \omega_c t/2\pi \lesssim 4300$. Trajectories are also shown in the $(v_z, v_\perp)$ plane (Fig. 16, right panels). The first and third test particles move roughly according to the conservation law $K=m_e(v_\perp^2/2\omega_c - n v_z/k_z)=cst$ [Eq. (11)]; the perpendicular velocities $v_\perp$ of the second particle (interactions at $n=0$) and of the third one (for $v_z \gtrsim -2$ and $\omega_c t/2\pi \gtrsim 4300$) are conserved.

V. CONCLUSION

The paper studies the nonlinear mechanisms at work in magnetized plasmas when wave packets with dense and almost continuous spectra interact resonantly with particle distributions presenting loss-cone-like structures. Lower hybrid waves are considered in view of the great importance, in space and laboratory plasmas, of waves with frequencies below the electron cyclotron frequency. Owing to a 3D self-consistent Hamiltonian model and a numerical symplectic code, the authors study the nonlinear stage of the loss-cone instability for various particle distributions and wave spectra, involving symmetric and asymmetric features.

At first, particle distributions and wave packets interacting at normal cyclotron resonances only are considered. Using single-sided loss-cone distributions, numerical simulations reveal that: (i) the first saturation stage of the wave energy growth due to particle trapping is followed by a sharper increase due to the process of dynamical resonance merging, that amplifies crucially the wave energies and leads to stochastic particle motion; (ii) the resonant electrons are accelerated along the magnetic field whereas their perpendicular kinetic energy decreases, the waves gaining partly the energy released by the particles; (iii) the filling of the loss-cone structure occurs in a time depending notably on the cone angle, leading to a near-equilibrium relaxed particle distribution that exchanges vanishingly small energy with most waves; (iv) for small values of the loss-cone angle θ_{lc}, the wave energy at saturation and the inverse of the cone filling time grow linearly with θ_{lc}^2; and (v) the motion of the resonant particles in the saturation stage is stochastic and does not reveal a classical diffusivelike character, showing that the phenomena observed cannot be fully described in the frame of the quasilinear theory of weak turbulence.

The dynamics of the wave-particle system becomes more complex when interactions not only at normal cyclotron resonances but also at Landau and anomalous cyclotron resonances can occur. In this case, distributions involving particles moving along the ambient magnetic field in both directions are considered. The presence of additional interaction resonances and mechanisms leads to the modification of the

energy and momentum transfers between the waves and the particles as well as of the asymptotic stage of the system's evolution and to the subsequent appearance of physical phenomena as particle acceleration and tail formation, wave damping, etc.

In order to provide a full description of the nonlinear processes at work, an exhaustive study is performed using various wave spectra and characteristic particle distributions: the single-sided loss-cone, the double-sided loss-cone, and the Maxwellian with loss-cone distributions; each case considered allows one to take simultaneously into account various kinds of interaction resonances and mechanisms. In the case of bilateral loss-cone distributions, the filling of the cone occurs as a result of wave-particle interactions at normal cyclotron resonances, as for the case of single-sided distributions; but an appreciable difference is revealed, which consists in the formation of a particle tail extending opposite to the magnetic field and resulting from interactions of particles with waves at Landau resonances as well as with beatings of some waves. For Maxwellian distributions with loss-cone structures, the wave-particle dynamics is more complex because interactions at anomalous cyclotron resonances responsible for the development of fan-type instabilities become essential and compete with loss-cone instabilities driven by normal cyclotron resonant interactions. It is shown that, for such distributions, the wave energy level at saturation is significantly increased, compared to single- and double-sided distributions with similar loss-cone structures and wave spectra.

ACKNOWLEDGMENTS

The authors acknowledge the Centre National de la Recherche Scientifique (PICS Grant No. 4960, CNRS, France), the Russian Academy of Sciences, and the Russian Foundation for Fundamental Research (Grant No. 09-02-91052) for their financial support. They thank Dr. Marie Flé (Direction Informatique, Université Paris Sud) for her technical support.

[1] D. E. Baldwin, Rev. Mod. Phys. **49**, 317 (1977).
[2] P. F. Mizera and J. F. Fennell, Geophys. Res. Lett. **4**, 311 (1977).
[3] D. R. Croley, P. F. Mizera, and J. F. Fennell, J. Geophys. Res. **83**, 2701 (1978).
[4] L. Eliasson, L. A. Homlgren, and K. Rönmark, Planet. Space Sci. **27**, 87 (1979).
[5] J. L. Phillips, W. C. Feldman, J. T. Gosling, C. M. Hammond, and R. J. Forsyth, in *Solar Wind Eight*, edited by D. Winterhalter *et al.* (American Institute of Physics, New York, 1996); AIP Conf. Proc. **382**, 293 (1996).
[6] O. Moullard, D. Burgess, C. Salem, A. Mangeney, D. E. Larson, and S. D. Bale, J. Geophys. Res. **106**, 8301 (2001).
[7] M. N. Rosenbluth and R. F. Post, Phys. Fluids **8**, 547 (1965).
[8] R. F. Post and M. N. Rosenbluth, Phys. Fluids **9**, 730 (1966).
[9] C. S. Wu and L. C. Lee, Astrophys. J. **230**, 621 (1979).
[10] E. Ungstrup, A. Bahnsen, H. K. Wong, M. André, and L. Matson, J. Geophys. Res. **95**, 5973 (1990).
[11] R. A. Dory, G. E. Guest, and E. G. Harris, Phys. Rev. Lett. **14**, 131 (1965).
[12] R. A. Treumann and W. Baumjohann, *Advanced Space Plasma Physics* (Imperial College Press, London, 1997).
[13] D. B. Melrose, *Instabilities in Space and Laboratory Plasmas* (Cambridge University Press, Cambridge, 1989).
[14] V. I. Karpman, Ju. K. Alekhin, N. D. Borisov, and N. A. Rjabova, Plasma Phys. **17**, 361 (1975).
[15] L. C. Lee and C. S. Wu, Phys. Fluids **23**, 1348 (1980).
[16] L. F. Ziebell, J. Plasma Phys. **39**, 431 (1988).
[17] W. A. Perkins and W. L. Barr, Phys. Fluids **11**, 388 (1968).
[18] J. A. Byers and M. Grewal, Phys. Fluids **13**, 1819 (1970).
[19] A. Zaslavsky, C. Krafft, and A. Volokitin, Phys. Plasmas **14**, 122302 (2007).
[20] J. Schneider, Phys. Rev. Lett. **2**, 504 (1959).
[21] J. L. Hirshfield and J. M. Wachtel, Phys. Rev. Lett. **12**, 533 (1964).
[22] M. J. Aschwanden, Astron. Astrophys. **237**, 512 (1990).
[23] P. L. Pritchett, Phys. Fluids **27**, 2393 (1984).
[24] P. L. Pritchett, Phys. Fluids **29**, 2919 (1986).
[25] J. S. Wagner, L. C. Lee, C. S. Wu, and T. Tajima, Geophys. Res. Lett. **10**, 483 (1983).
[26] J. S. Wagner, L. C. Lee, C. S. Wu, and T. Tajima, Radio Sci. **19**, 509 (1984).
[27] L. F. Ziebell and P. H. Yoon, Phys. Plasmas **2**, 1285 (1995).
[28] H. Okuda and A. Hasegawa, Phys. Fluids **12**, 676 (1969).
[29] Y. Omura and H. Matsumoto, J. Geophys. Res. **92**, 8649 (1987).
[30] M. Ashour-Abdalla, J. N. Leboeuf, J. M. Dawson, and C. F. Kennel, Geophys. Res. Lett. **7**, 889 (1980).
[31] T. Umeda, M. Ashour-Abdalla, D. Schriver, R. L. Richard, and F. V. Coroniti, J. Geophys. Res. **112**, A04212 (2007).
[32] W. S. Kurth, L. A. Frank, M. Ashour-Addalla, D. A. Gurnett, and B. G. Burek, Geophys. Res. Lett. **7**, 293 (1980).
[33] W. S. Kurth, J. D. Craven, L. A. Frank, and D. A. Gurnett, J. Geophys. Res. **84**, 4145 (1979).
[34] K. Rönnmark, H. Borg, P. J. Christiansen, M. P. Gough, and D. Jones, Space Sci. Rev. **22**, 401 (1978).
[35] A. Volokitin and C. Krafft, Phys. Plasmas **11**, 3165 (2004).
[36] C. Krafft, A. Volokitin, and A. Zaslavsky, Phys. Plasmas **12**, 112309 (2005).
[37] C. Krafft and A. Volokitin, Phys. Plasmas **13**, 122301 (2006).
[38] C. Krafft and A. Volokitin, Ann. Geophys. **22**, 2171 (2004).
[39] A. Zaslavsky, C. Krafft, and A. Volokitin, Phys. Rev. E **73**, 016406 (2006).
[40] A. A. Vedenov, E. P. Velikhov, and R. Z. Sagdeev, Nucl. Fusion **2**, (Suppl.), 465 (1962).
[41] W. E. Drummond and D. Punes, Nucl. Fusion **3**, 1049 (1962).
[42] A. B. Kitsenko, I. M. Pankratov, and K. N. Stepanov, Sov. Phys. JETP **40**, 860 (1974).
[43] J. R. Cary and I. Doxas, J. Comput. Phys. **107**, 98 (1993).
[44] J. M. Sanz-Serna and M. P. Calvo, *Numerical Hamiltonian Problems* (Chapman and Hall, London, 1994).
[45] Y. Elskens and D. Escande, *Microscopic Dynamics of Plasmas and Chaos* (Institute of Physics, University of Reading, Berkshire, 2003).
[46] B. Chirikov, Phys. Rep. **52**, 263 (1979).